HHS Public Access

Author manuscript

IOP Conf Ser Mater Sci Eng. Author manuscript; available in PMC 2021 September 27.

Published in final edited form as:

IOP Conf Ser Mater Sci Eng. 2020 ; 756: . doi:10.1088/1757-899x/756/1/012018.

The Role of CHPD and AIMI processing on enhancing J_C and transverse connectivity of *in-situ* MgB_2 strand

F Wan[1], **M D Sumption**[1], **M A Rindfleisch**[2], **E W Collings**[1]

[1]Center for Superconductor and Magnetic Materials, Department of Materials Science and Engineering, The Ohio State University, Columbus, OH 43210, USA.

[2]Hyper Tech Research Inc, Columbus, OH 43228, USA

Abstract

Research into *in-situ* MgB_2 strand has been focused on improvements in J_C through reduction of porosity. Both of cold-high-pressure-densification (CHPD) and advanced-internal-magnesium-infiltration (AIMI) techniques can effectively remove the voids in *in-situ* MgB_2 strands. This study shows the nature of the reduced porosity for *in-situ* MgB_2 strands lies on increases in transverse grain connectivity as well as longitudinal connectivity. The CHPD method bi-axially applying 1.0 GPa and 1.5 GPa yielded 4.2 K $J_{CM||}$s of 9.6×10^4 A/cm^2 and 8.5×10^4 A/cm^2 at 5 T, respectively, with compared with 6.0×10^4 A/cm^2 for typical powder-in-tube (PIT) *in-situ* strand. Moreover, AIMI-processed monofilamentary MgB_2 strand obtained even higher J_Cs and transverse grain connectivity than the CHPD strands.

1. Introduction

MgB_2 superconducting strands are promising to the practical magnetic application due to its high transition temperature T_C (39 K) [1], high coherence length [2, 3], and low anisotropy of upper critical fields (B_{c2}) [3–6]. The powder-in-tube (PIT) *in-situ* MgB_2 strands were fabricated by filling a mixture of Mg and B powder into a non-reactive metallic tube and then being cold-worked into wires or tapes. The PIT strands have large amount of voids elongated along longitudinal strand axis which were left behind by molten Mg powders after heat treatment [7]. The present of voids tends to limit the number of the continuous current path in the *in-situ* MgB_2 strand and therefore suppress the current-carrying-capacity of the strand.

The CHPD technique can effectively increase the transport properties of PIT *in-situ* MgB_2 strands by eliminating the pores [8–11]. The pre-reacted powder-in-tube composite was bi-axially cold-densified at room temperature to increase the mass density of the Mg + B mixture. In this case, the cold-densified MgB_2 strand can obtain higher grain connectivity after heat treatment. Additionally, the Mg reactive – liquid – infiltration (RLI) process,

Corresponding author: wan.108@osu.edu.

initiated by Giunchi *et al* [12], also has the ability to eliminate the pores and produce a dense MgB_2 layers in *in-situ* MgB_2 strands. For RLI process, a Mg rod is inserted axially into a boron-filled metallic tube. After wire drawing the heat treatment (H. T.), MgB_2 layer is formed through the reactive diffusion of Mg into B layer. Since Mg is totally separated with precursor B layer before H. T., the RLI process can totally eliminate the "Mg-site porosity" from MgB_2 layer but induce the formation of a big hole at the central region of the strand [13]. Furthermore, since the molar volume of MgB_2 (17.46 cm^3/mol) is twice as that of two B atoms (9.18 cm^3/mol), the volume expansion associated with the reactive transformation from 2B to MgB_2 enables even better connections between MgB_2 grains during heat treatment [13]. Our group named our RLI-processed strands as advanced – internal – magnesium – infiltration (AIMI) strands due to their optimized strand architecture and high J_Cs [13].

The previous researches mostly focused on investigating the effect of CHPD and AIMI techniques on the transport properties along longitudinal strand axis of *in-situ* MgB_2 strands, such as transport J_Cs and longitudinal grain connectivity. However, Shi and Susner pointed out that high anisotropic grain connectivity exists in PIT *in-situ* strands, which was resulted from the elongated voids between elongated MgB_2 stringers [7]. Therefore longitudinal transport properties are different with the transport properties along transverse strand axis for MgB_2 superconducting wires. In continuing along these lines, the transport properties along transverse strand axis were investigated for the 2.0 mol% C-doped *in-situ* MgB_2 strands in this study. The anisotropic connectivity of the PIT strands results in the differences between perpendicular magnetic J_C ($J_{CM\_|\_}$) and parallel J_C ($J_{CM\parallel}$). The influence of aspect ratio (S = length/diameter) on transverse and longitudinal J_C were investigated for the PIT strand (P00). The CHPD-processed strands were P10 (1.0 GPa cold-pressing) and P15 (1.5 GPa cold-pressing). According to the previous results of our group, the CHPD technique increased the transport J_C of the monofilamentary PIT *in-situ* MgB_2 strand from 3.0×10^4 A/cm^2 to 3.6×10^4 A/cm^2 at 4.2 K and 10 T due to decreased porosity [11] and AIMI-processed MgB_2 strands attained the 4.2 K, 10 T transport layer J_Cs of $1.0 \sim 1.5 \times 10^5$ A/cm^2 [13–16]. In this study, we compared the $J_{CM\parallel}$s and transverse connectivity of the CHPD- and AIMI-processed strands with those of the P00 strand at 4.2 K and 20 K. The relationship between porosity and transverse flux pinning force density $F_{p\parallel}$, which is $J_{CM\parallel} \times B$, for the *in-situ* MgB_2 strands was also discussed.

2. Experimental

2.1. Sample preparation

A series of pre-reacted powder-in-tube (PIT) *in-situ* strands, typically 0.834 mm diameter, with a Nb barrier and a Cu outer sheath were fabricated by Hyper Tech Research, Inc. (HTR). Two PIT strands (designated P10 and P15) were bi-axially densified with 1.0 GPa and 1.5 GPa at room temperature, respectively. The other strand (designed A00) manufactured through AIMI technique were also provided by HTR. The AIMI-processed strand, with 0.55 mm diameter, has a Nb barrier and a Monel outer sheath. The powders used for the present strands were 2 mol% C–doped amorphous B (10 – 100 nm) from Specialty Materials Inc. (SMI). The cold–densified PIT strands were heat-treated at 675 °C

for 1 h and the AIMI strand was heat – treated at 625 °C for 16 h. The specification and heat treatment (H. T.) conditions of the strands are presented in table 1.

2.2. Transport and Magnetic Measurements

The transport I_C (I_{CT}) test was conducted in perpendicular magnetic field up to 13 T in a pool of liquid Helium at 4.2 K on the MgB_2 strands with a total length of 50 mm and a gauge length of 5 mm. The electric criterion used for determining I_{CT}s is 1.0 μV/cm. The magnetizations versus perpendicular and parallel magnetic fields ($M-H$) loops were measured by a Quantum Design Model 6000 Physical Property Measuring System (PPMS) for all strands with a sample length of 3 – 5 mm.

3. Results

The J_{CT}s of the PIT strands were the transport critical current normalized by MgB_2 core area. As shown in Figure 1(a) the MgB_2 core of the typical PIT *in-situ* strand is a solid cylinder. Figure1(b)–(d) shows the shape of MgB_2 cores for the CHPD- and AIMI-processed strands are cuboid and hollow cylinder, respectively. The J_{CT} of the AIMI–processed strands, which is also named as transport layer J_C, were calculated by dividing the I_{CT} by the area of annulus MgB_2 layer. Values of magnetic J_C ($J_{CM\_|\_}$ and $J_{CM\|}$) for the MgB_2 strands were extracted from the full $M-H$ loops heights ΔM, using the standard Bean model equations [7, 17]:

For the PIT *in–situ* wire P00:

$$\text{Perpendicular Magnetic } J_C\text{: } J_{CM\_|\_} = \frac{3\pi\Delta M}{8R_0} \tag{1}$$

$$\text{Parallel Magnetic } J_C\text{: } J_{CM\|} = \frac{3\Delta M}{2R_0} \tag{2}$$

Here R_0 is the radius of the cylinder MgB_2 core in the PIT wire.

For the densified wires P10 and P15:

$$\text{Parallel Magnetic } J_C\text{: } J_{CM\|} = \frac{2\Delta M}{b\left(1-\frac{b}{3a}\right)} \tag{3}$$

Here a, b are both lengths of the transverse cross – sectional area of cuboid MgB_2 core, a > b.

For the AIMI wire A00:

$$\text{Parallel Magnetic } J_C\text{: } J_{CM\|} = \frac{3\Delta M}{2}\frac{R_0^2-R_i^2}{R_0^3-R_i^3} \tag{4}$$

Here R_i is the inner diameter of the annulus MgB_2 layer and R_0 is the outer diameter of the annulus MgB_2 layer.

3.1. Transport and magnetic critical current densities, J_{CT} and J_{CM}

Figure 2(a) shows the J_{CT} and $J_{CM\_|\_}$ versus B at 4.2 and 20 K for the strand P00. It can be seen that $J_{CM_|_}$s agree with J_{CT} at low fields, whereas the bifurcation of J_{CT} and $J_{CM\_|\_}$ happened at high fields. Moreover, $J_{CM_|_}$s were greatly affected by the aspect ratio S, especially at high magnetic fields. The relationships among J_{CT}, $J_{CM\_|\_}$, and aspect ratio were fully discussed in ref [7] and [18]. Therefore, the values of $J_{CM\_|\_}$ are not only determined by the intrinsic properties but also the extrinsic properties of the *in-situ* MgB_2 strands. As shown in Figure 2(b) $J_{CM\|}$s were independent on the aspect ratio S. Based on this result, we can know the values of $J_{CM\|}$s as well as J_{CT}s are merely determined by the intrinsic properties of the *in-situ* MgB_2 strands. The MgB_2 macrostructure of the reacted PIT *in-situ* strand is characterized by elongated polycrystalline MgB_2 fibers and elongated pores partially separating the fibers [7, 11, and 18]. The J_{CT}s and $J_{CM\|}$s can represent the longitudinal and transverse connectivity of the MgB_2 fibers, respectively. In summary, we can investigate the effect of CHPD and AIMI technique on the current–carrying–capacity of the *in–situ* MgB_2 strands through $J_{CM\|}$s as well as J_{CT}.

Figure 3 shows the J_{CT} and $J_{CM\|}$ versus B at 4.2 and 20 K for all strands. The CHPD technique significantly enhanced $J_{CM\|}$s of PIT *in-situ* strands at 4.2 K. Strand P10 and P15 attained 9.5×10^4 A/cm^2 and 8.5×10^4 A/cm^2 at 4.2 K and 5 T, with respect to 6.0×10^4 A/cm^2 for strand P00. 4.2 K J_{CT}s were slightly enhanced by the CHPD technique. Therefore, the increases in J_{CT} and $J_{CM\|}$ indicated that the both longitudinal and transverse connections between MgB_2 fibers were enhanced. With the formation of high density MgB_2 layer, strand A00 attained 4.2 K, 10 T J_{CT} of 9.4×10^4 A/cm^2, which is 180% higher than those of CHPD-processed strands. On the other hand, the AIMI strand obtained 5 T $J_{CM\|}$s of 3.1×10^5 A/cm^2 at 4.2 K and 1.7×10^4 A/cm^2 at 20 K, which are about 240% higher than those of CHPD strands.

3.2. Transverse Flux Pinning, Porosity and Transverse Grain Connectivity

Figure 4 shows the $F_{p\|}/F_{p,max\|}$ versus B/B_{irr} for all strands, where $F_{p\|} = J_{CM\|} \times B$. It can be seen that the peak pinning occurred at $b = B/B_{irr\|}$ close to 0.2 at 4.2 and 20 K, which is in agreement with the Dew-Hughes/Kramer model [19, 20]. In other words, the dominant pinning centers for the all strands are also grain boundaries for the direction along transverse strand axis. According to the previous work [11], the densified wires have decreased porosities, the values of porosity are ~ 50% (p = 0) and ~ 30 % (p = 1.0 or 1.5 GPa). Since the Mg–site porosity was totally eliminated for AIMI–processed strands, the porosity of the AIMI strand is close to 0. Therefore, both CHPD and AIMI processes enable the resulting MgB_2 phases to be denser and more connected. For the discussion, it can be concluded that the enhanced J_{CT} and $J_{CM\|}$ in densified wires and AIMI wire is correlated with lower porosity (higher grain connectivity).

The connectivity K defined by Rowell [21] can represent the grain connectivity of MgB_2 strands. The connectivity K is calculated by the equation:

$$K = \frac{\Delta\rho_{SC}}{\Delta\rho} \tag{5}$$

Here $\Delta\rho$ is the difference between the sample's resistivity at 300 K and the sample's resistivity at 40 K and $\Delta\rho_{SC}$ is the resistivity difference for an ideal single crystal. However, transverse connectivity $K_{\parallel}$ is difficult to be determined for the MgB_2 wires. It has been reported that the maximum flux pinning force densities of fully–connected MgB_2 superconductor, where grain connectivity K = 100 %, are estimated to be 90 GN/m^3 at 4.2 K and 22 GN/m^3 at 20 K [22]. Therefore, we can roughly estimate the transverse grain connectivities $K_{\parallel}$s of the *in-situ* MgB_2 strands by normalizing the $F_{p,max\parallel}$ with the $F_{p,max}$ of fully-connected MgB_2. Table 2 shows the transverse maximum flux pinning force densities $F_{p,max\parallel}$ at 4.2 K and 20 K and estimated transverse grain connectivities for all the strands. The connectivity of 5% is achieved by the 2 mol% C-doped PIT strand, P00. The cold–densification increases the connectivity of PIT strand by 20 %. The AIMI strand A00 obtained the highest transverse grain connectivities of 20 %.

4. Conclusion

$J_{CM\parallel}$s is merely determined by the intrinsic properties of *in-situ* MgB_2 strands, so the current-carrying capacity of *in-situ* MgB_2 strands can be represented by $J_{CM\parallel}$ as well as J_{CT}. The CHPD of 1.0 GPa and 1.5 GPa enhanced the 4.2 K, 5 T $J_{CM\parallel}$ from 6.0 × 10^4 A/cm^2 to 9.6 × 10^4 A/cm^2 and 8.5 × 10^4 A/cm^2, respectively. AIMI strand attained the highest J_{CT} and $J_{CM\parallel}$ at 4.2 and 20 K due to the formation of a high dense MgB_2 layer. By eliminating the voids in *in-situ* MgB_2 strands through CHPD and AIMI technique, better connections between MgB_2 grains along transverse strand axis can be obtained in *in–situ* MgB_2 strands

5. References

[1]. Nagamatsu J, Nakagawa N, Muranaka T, Zenitani Y, and Akimitsu J2001Nature41063–64 [PubMed: 11242039]

[2]. Finnemore DK, Ostenson JE, Bud'ko SL, Lapertot G and Canfield PC 2001 Rhys. Rev. Lett 86 2420–2422

[3]. Vinod K, Abhilash Kumar RG and Syamaprasad U 2007 Supercond. Sci. Technol 20 R1–R3

[4]. Eltsev Y, Lee S, Nakao K, Chikumoto N, Tajima S, Koshizuka N and Murakami M 2002 Phys. Rev. B 65 140501

[5]. Eisterer M, Zehetmayer M and Weber HW 2003 Phys. Rev. Lett 90 247002 [PubMed: 12857216]

[6]. De Liam OF, Ribeiro RA, Avila MA, Cardoso CA and Coelho AA 2001 Phys. Rev. Lett 86 5974 [PubMed: 11415407]

[7]. Shi ZX, Susner MA, Majoros M, Sumption MD, Peng X, Rindfleisch M, Tomsic MJ and Collings EW 2010 Supercond. Sci. Technol 23 045018

[8]. Flukiger R, Hossain MSA and Senatore C 2009 Supercond. Sci. Technol 22 085002

[9]. Hossain MSA, Senatore C, Flukiger R, Rindfleisch MA, Tomsic MJ, Kim JH and Dou SX 2009 Supercond. Sci. Technol 22 095004

[10]. Hossain MSA. et al. 2014; Supercond. Sci. Technol. 27 :095016.

[11]. Wan F, Sumption MD, Rindfleisch MA and Collings EW 2017 IOP Conf. Series: Materials Science and Engineering 279 012024

[12]. Giunchi G, Ripamonti G, Perini E, Cavallin T and Bassani E 2007 IEEE TRANSACTIONS ON APPLIED SUPERCONDUCTIVITY 17 2761

[13]. Li GZ, Sumption MD, Susner MA, Yang Y, Reddy KM, Rindfeisch MA, Tomsic MJ, Thong CJ and Collings EW 2012 Supercond. Sci. Technol 25 115023

[14]. Ye SJ, Matsumoto A, Zhang YC and Kumakura H 2014 Supercond. Sci. Technol 27 085012

[15]. Li GZ, Sumption MD, Zwayer JB, Susner MA, Rindfleisch MA, Thong CJ, Tomsic MJ and Collings EW 2013 Supercond. Sci. Technol 26 095007

[16]. Kumakura H, Hur J, Togano K, Matsumoto A, Wada H and Kimura K 2011 IEEE Trans. Appl. Supercond 21 2643

[17]. Sumption MD, Peng X, Lee X, Wu X and Collings EW 2004 Cryogenics 44 711–725

[18]. Susner MA, Daniels TW, Sumption MD, Rindfleisch MA, Thong CJ and Collings EW 2012 Supercond. Sci. Technol 25 065002

[19]. Dew-Hughes D1974Philos. Mag30293–305

[20]. Kramer EJ1973J. Appl. Phys441360–70

[21]. Rowell J2003Supercond. Sci. Technol16R17–27

[22]. Matsushita T, Kiuchi M, Yamamoto A, Shimoyama J and Kishio K 2008 Physica C 468 1833

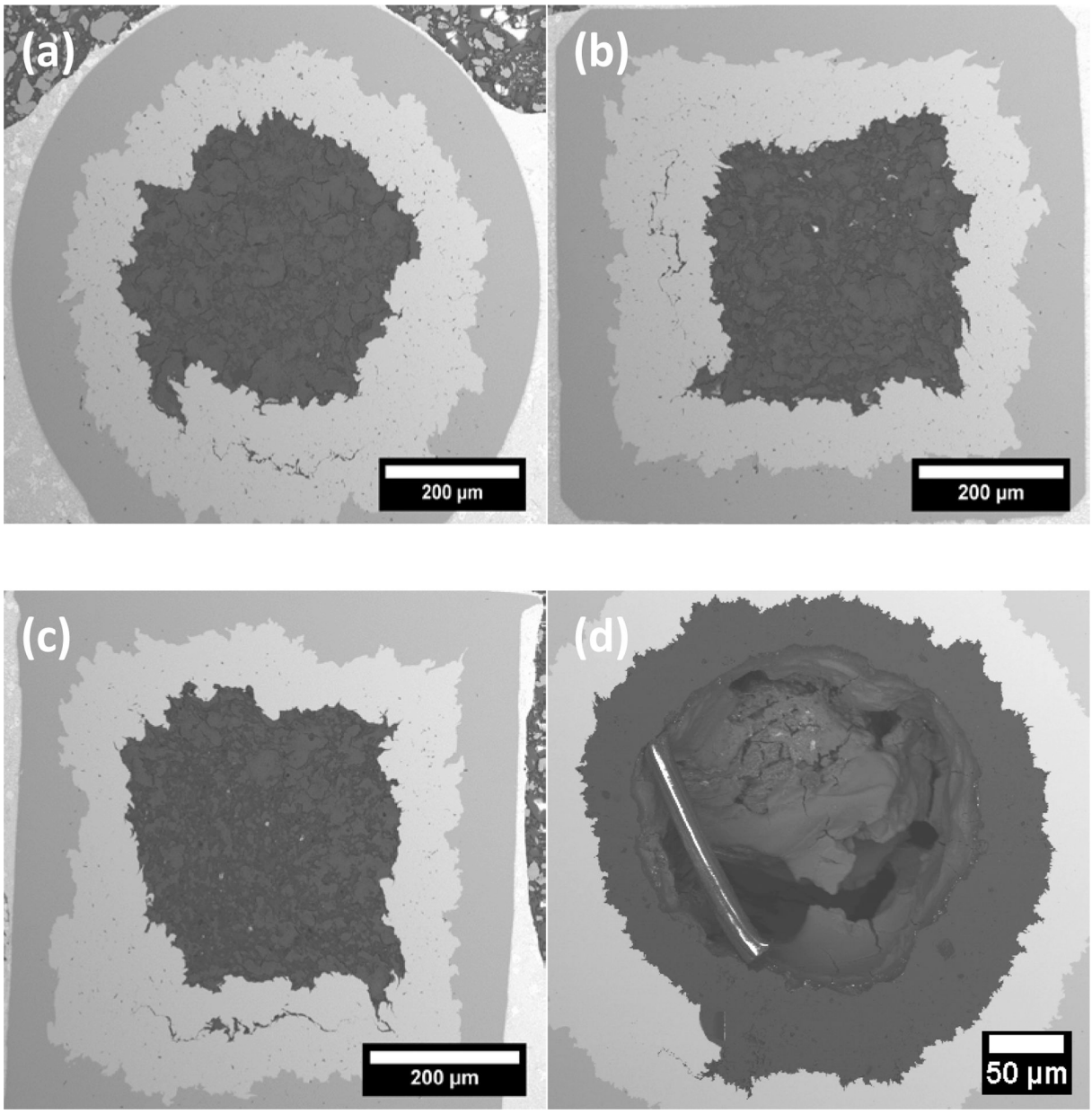

Figure 1.

(a) Back scattered SEM images of (a) strand P00, (b) strand P10 (1.0 GPa cold pressure), (c) strand P15 (1.5 GPa cold pressure), and (d) AIMI strand A00.

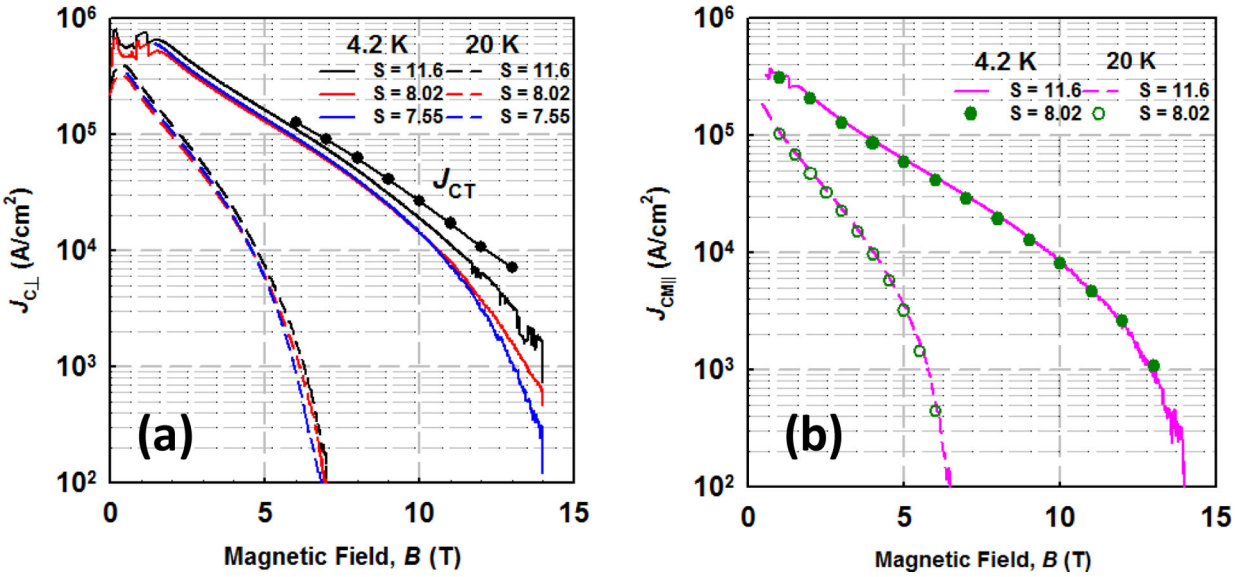

Figure 2.

(a) J_{CT} and $J_{CM\_|\_}$ versus B at 4.2 and 20 K (b) $J_{CM\parallel}$ versus B at 4.2 and 20 K for strand P00

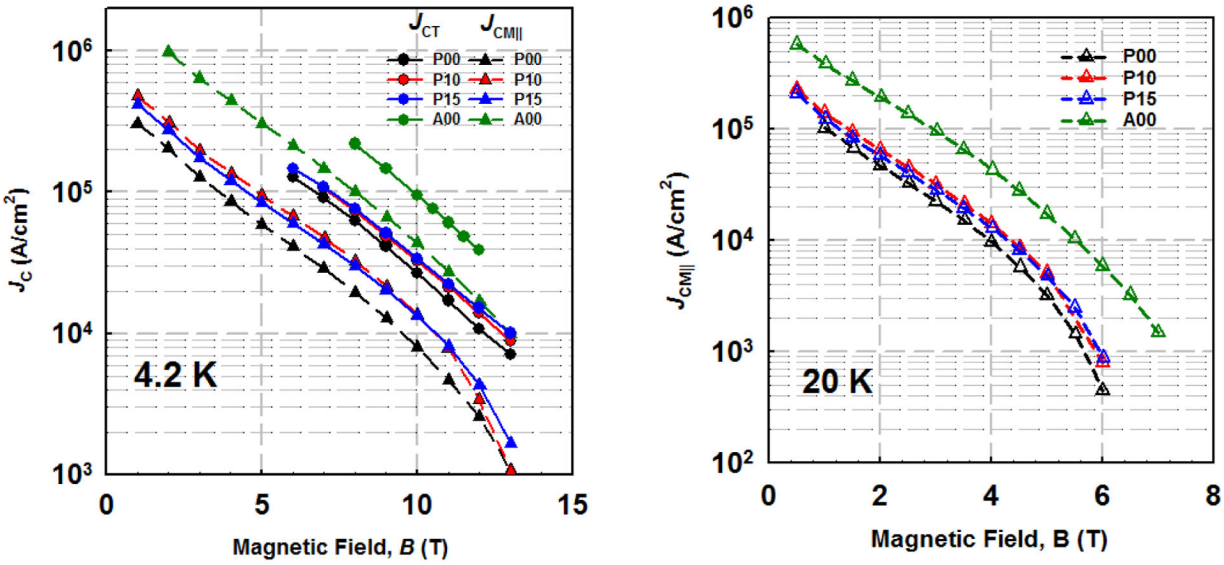

Figure 3.

J_{CT} and $J_{CM||}$ versus B at 4.2 and 20 K for all strands

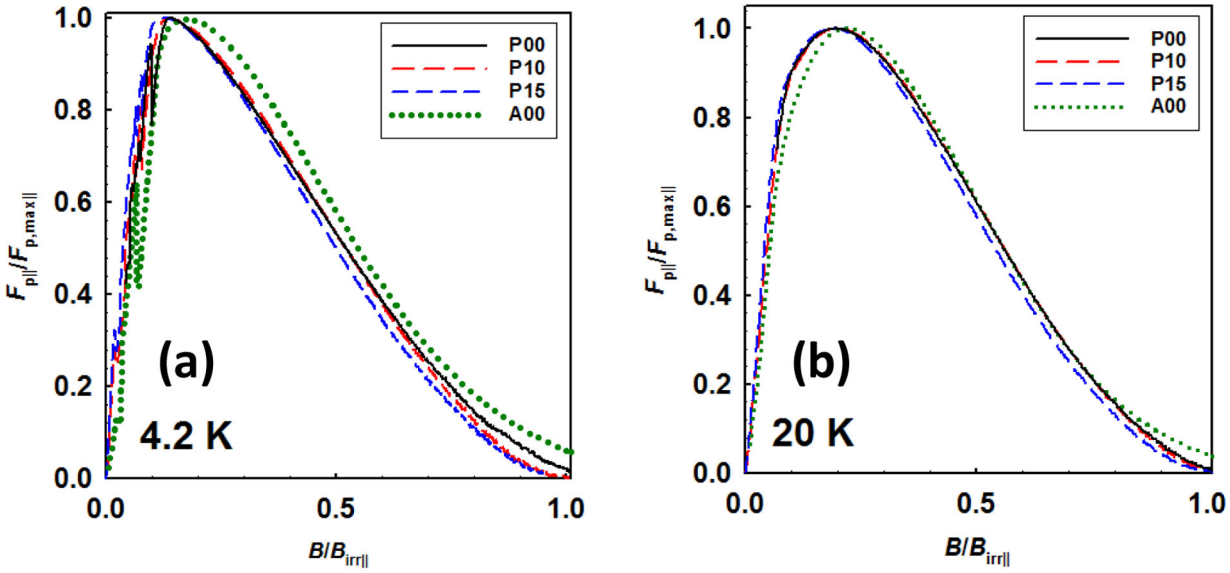

Figure 4.

(a) $F_{p||}/F_{p,max||}$ versus B/B_{irr} for all strands at 4.2 K, (b) $F_{p||}/F_{p,max||}$ versus B/B_{irr} for all strands at 20K

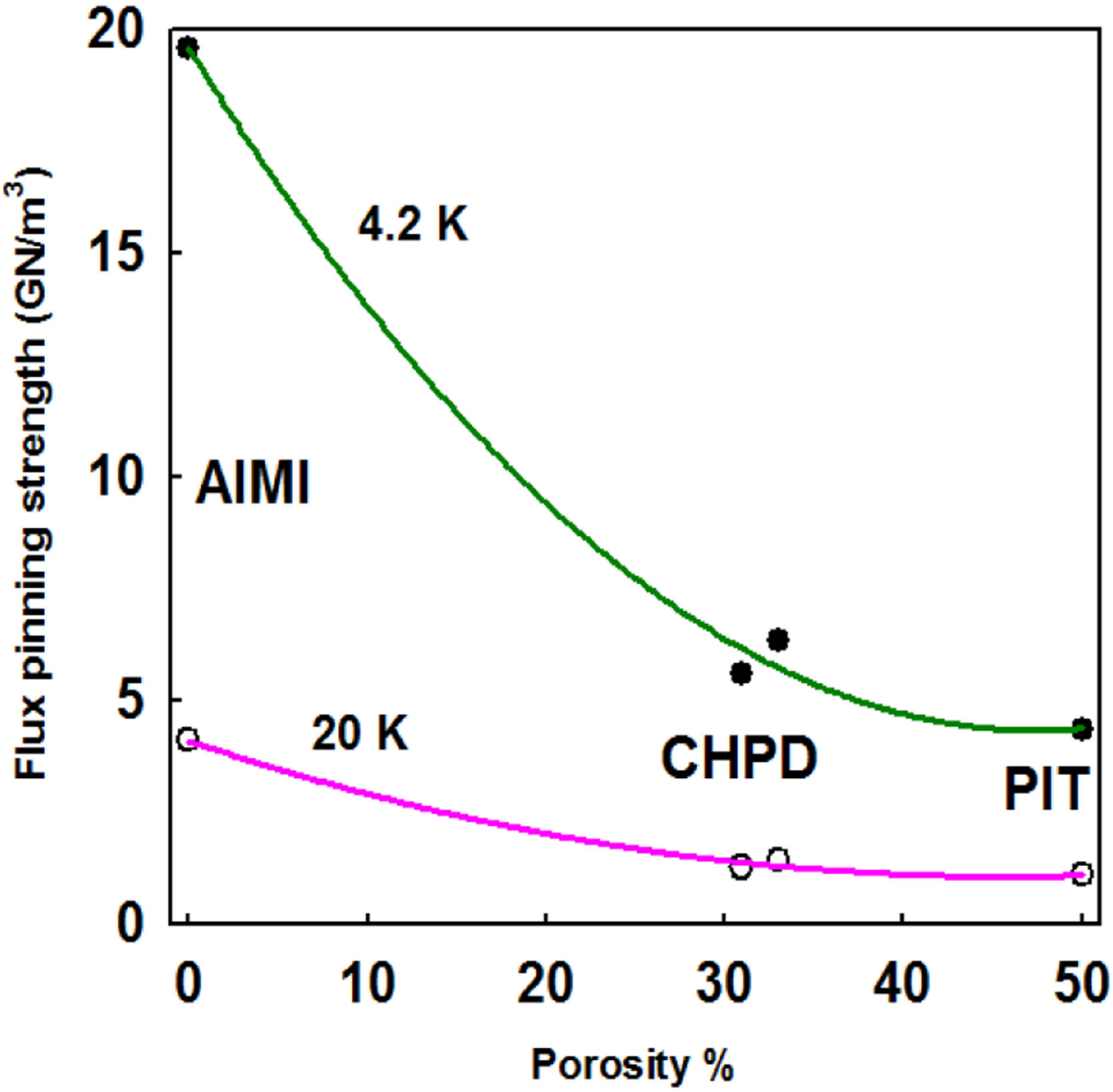

Figure 5.
Relationship between porosity and transverse flux pinning force densities for *in–situ* MgB_2 strands

Table 1.

Strand specification and H. T. conditions

Strand Name	Strand Type	CHPD (GPa)	H. T. (h/°C)
P00	PIT	0.0	1/675
P10	PIT	1.0	1/675
P15	PIT	1.5	1/675
A00	AIMI	0.0	16/625

Table 2.

Transverse flux pinning force densities and estimated connectivity of the strands.

Strand Name	$F_{p,max∥}$, 4.2 K (GN/m^3)	$F_{p,max∥}$, 20 K (GN/m^3)	Transverse Connectivity, $K_∥$ %
P00	4.3	1.1	5.0
P10	6.3	1.4	6.0
P15	5.6	1.3	6.0
A00	19.6	4.1	20